iScience

CellPress
OPEN ACCESS

Article

Electrochemical transformation of limestone into calcium hydroxide and valuable carbonaceous products for decarbonizing cement production

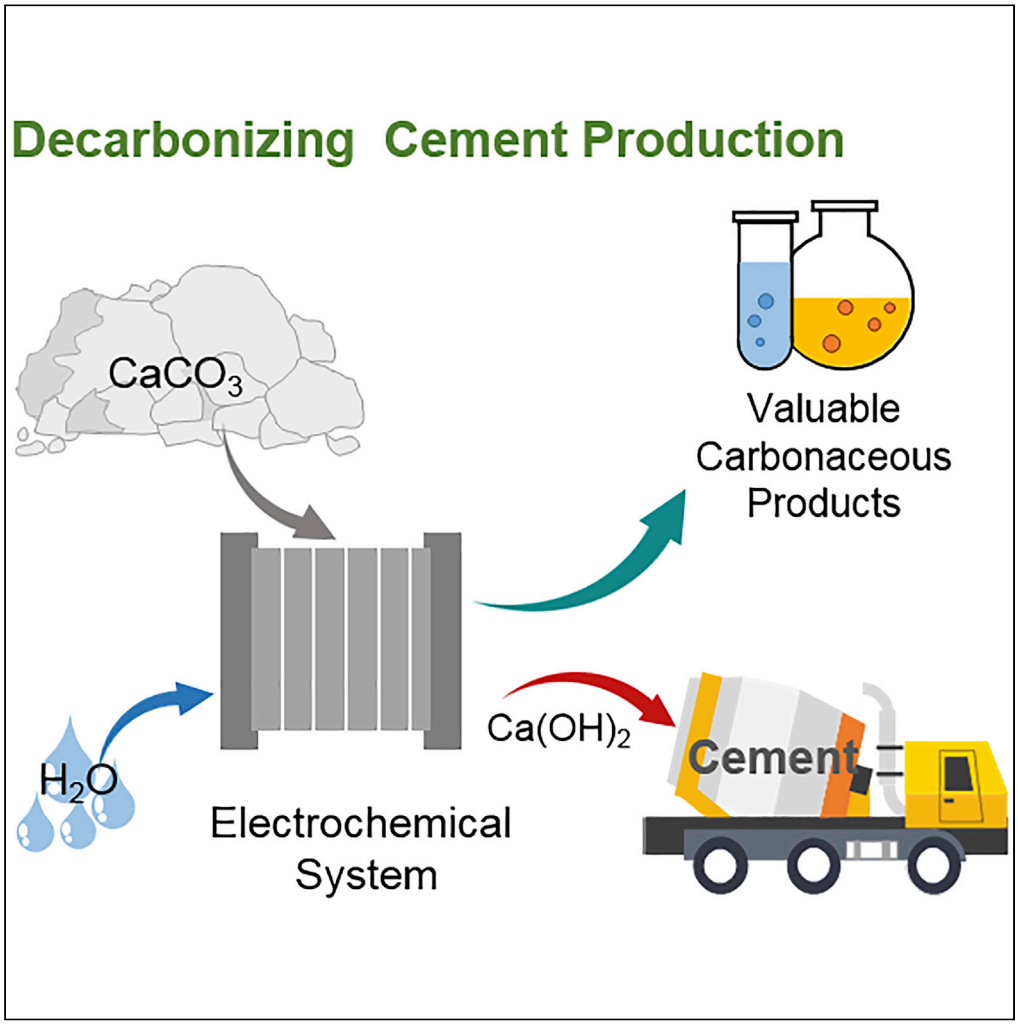

Qixian Xie, Lili Wan, Zhuang Zhang, Jingshan Luo

jingshan.luo@nankai.edu.cn

Highlights

An electrochemical process transforms $CaCO_3$ into $Ca(OH)_2$ and carbonaceous products

The FE of CO and formate of this process could be achieved at ~20%

Alkenes and alkanes could be generated based on the conversion of $CaCO_3$

Demonstrated a green and sustainable manner for the cement industry

Xie et al., iScience 26, 106015
February 17, 2023
https://doi.org/10.1016/j.isci.2023.106015

iScience

CellPress
OPEN ACCESS

Article

Electrochemical transformation of limestone into calcium hydroxide and valuable carbonaceous products for decarbonizing cement production

Qixian Xie,[1] Lili Wan,[1] Zhuang Zhang,[1] and Jingshan Luo[1,2,3,*]

SUMMARY

The cement industry is one of the largest contributors to global CO_2 emissions, which has been paid more attention to the research on converting the CO_2 released by the cement production process. It is extremely challenging to decarbonize the cement industry, as most CO_2 emissions result from the calcination of limestone ($CaCO_3$) into CaO and CO_2. In this work, we demonstrate an *in situ* electrochemical process that transforms $CaCO_3$ into portlandite ($Ca(OH)_2$, a key Portland cement precursor) and valuable carbonaceous products, which integrates electrochemical water splitting and CO_2 reduction reaction with the chemical decomposition of $CaCO_3$. With different metal catalyst electrodes (like Au, Ag, In, Cu, and Cu nanowires electrodes), we have achieved various valuable carbonaceous products, such as CO, formate, methane, ethylene, and ethane during the electrochemical CO_2 process. Our work demonstrates a proof of concept for green and sustainable cement production.

INTRODUCTION

Since the industrial revolution, the rapid increase in global energy demand and human activities has greatly increased the CO_2 concentration in the atmosphere, leading to global warming.[1–4] The cement industry for building materials is one of the largest CO_2 emission sources, accounting for ~7% of global CO_2 emissions.[5,6] The production of one ton of cement emits 561–622 kg of CO_2, which is emitted from the decomposition of limestone ($CaCO_3$) to CaO (~60%), the combustion of fossil fuels for heating (~30%), and the power consumption for the associated equipments (~10%).[5–9] The latter two energy consumption pathways can be easily switched to renewable energy for carbon neutrality, but the elimination of CO_2 emission during the decomposition of $CaCO_3$ into CaO still faces a substantial challenge. Currently, the pressure of decarbonation is prompting efforts to reimagine the future of disruptive technologies.

Recently, Fennell et al. discussed the potential to decarbonize cement production by improving energy efficiency, developing alternative materials, and adjusting the production process.[5] Chiang et al. demonstrated the electrochemical synthesis of cement by transforming $CaCO_3$ and water into $Ca(OH)_2$ via Pt electrodes (Table S1), which could be driven by renewable electricity.[7] They proposed that the CO_2 could be directly captured and sequestered. Based on $CaCO_3$, Zenyuk et al. demonstrated a flow-through concept for $Ca(OH)_2$ production via a bipolar membrane (BPM) CO_2 electrolyzer.[10] In addition, Guan et al. demonstrated the use of electrochemical pH gradients for direct air capture with a calcium-based loop, which enabled simultaneous CO_2 capture and carbonate regeneration.[11] However, no further research on CO_2 utilization was investigated. Furthermore, Berlinguette's group used a BPM electrolysis system to directly reduce bicarbonate solution into C_1 products, like CO, formate, etc.[12,13] The system first generated H^+, which reacted with the $KHCO_3$ solution to release CO_2, and then the generated CO_2 was further reduced.[14–16] Moreover, they also reported an electrochemical flow electrolyzer via Ni electrodes (Table S1), which could continuously convert $CaCO_3$ into $Ca(OH)_2$ at a high rate of product formation and decrease the amount of CO_2 emitted per tonne of cement by 75%.[17]

Inspired by the works above,[5,7,10,17] here, we propose an integrated process for cement production via the electrochemical pulsed method, which converts $CaCO_3$ into $Ca(OH)_2$ and valuable carbonaceous products. Different from the previous reports,[7,17] our work *in situ* converts the CO_2 generated via $CaCO_3$ dissolution into valuable carbonaceous products, which demonstrates a proof of concept for cement production

[1]Institute of Photoelectronic Thin Film Devices and Technology, Solar Energy Research Center, Key Laboratory of Photoelectronic Thin Film Devices and Technology of Tianjin, Ministry of Education Engineering Research Center of Thin Film Photoelectronic Technology, Renewable Energy Conversion and Storage Center, Nankai University, Tianjin 300350, China

[2]Haihe Laboratory of Sustainable Chemical Transformations, Tianjin 300192, China

[3]Lead contact

*Correspondence: jingshan.luo@nankai.edu.cn

https://doi.org/10.1016/j.isci.2023.106015

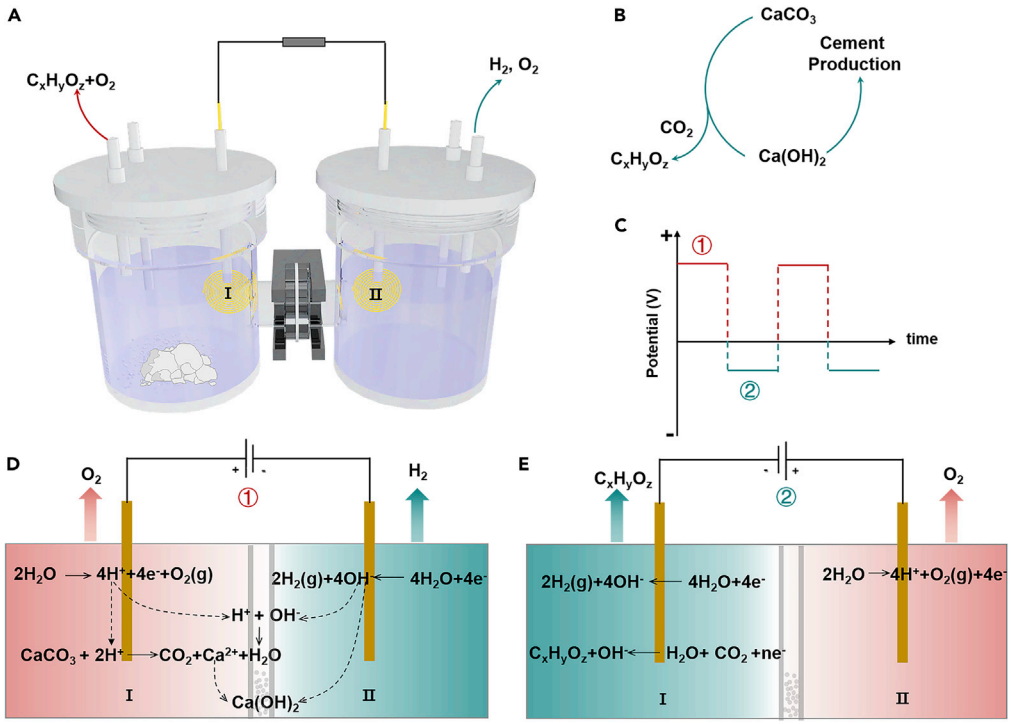

Figure 1. Scheme of the electrochemical transformation process of $CaCO_3$ into $Ca(OH)_2$ and valuable carbonaceous products

(A) Schematic diagram of the electrochemical cell for converting $CaCO_3$ into $Ca(OH)_2$ and valuable carbonaceous products.

(B) The cycle of $CaCO_3$ converting to $Ca(OH)_2$ and valuable carbonaceous products.

(C) The scheme of pulsed chronopotentiometry method for the electrochemical process.

(D) The reaction process of the transformation of $CaCO_3$ into $Ca(OH)_2$ and CO_2.

(E) The conversion process of the generated CO_2 into valuable carbonaceous products.

without CO_2 emission. Moreover, this design enables *in situ* conversion of CO_2 during cement production. The process first uses electrochemical water splitting to generate H^+, which decomposes $CaCO_3$ into $Ca(OH)_2$ and CO_2[7]. The pH of the electrolyte after the oxygen evolution reaction (OER) process for 20 min was tested via the pH meter, which is 5.27 (Figure S1). Then, the CO_2 is *in situ* electrochemically reduced to valuable carbonaceous products via an electrochemical CO_2 reduction process. As previous literature point out, the resulting $Ca(OH)_2$ can react with SiO_2 to synthesize cement.[7,18] Here, different metal catalyst electrodes (like Au, Ag, In, Cu, and Cu nanowires electrodes) were used as electrodes for the electrochemical CO_2 reduction process. In a two-chamber electrochemical cell, ~20% Faradaic efficiency (FE) of CO at an applied current of −3 mA with a Au electrode (electrode area, 0.78 cm^{-2}) was achieved using $CaCO_3$ as a carbon source. Moreover, based on a triple-chamber electrochemical cell, different carbonaceous products such as formate, methane, ethylene, and ethane were obtained via the In and Cu-based electrocatalysts, depending on the selectivity of the electrocatalysts.

RESULTS AND DISCUSSION

The electrochemical transformation process of $CaCO_3$ into $Ca(OH)_2$ and valuable carbonaceous products integrates electrochemical water splitting and CO_2 reduction reaction with the chemical decomposition of $CaCO_3$ (Figures 1A–1C). First, a positive current is applied at electrode I in left chamber (L), process 1, as shown in Figure 1C. Therefore, the OER and the hydrogen evolution reaction (HER) happened in the left (L) chamber and right (R) chamber, respectively, Figure 1D; the detailed processes were shown in Equations (1, 2, 3, and 4), which is partially similar to the work reported by Chiang et al.[7] Here, the electrolyte is $NaClO_4$, which constructs neutral condition, H^+ is generated in chamber L, and OH^- is generated in chamber R, as shown in Equations (1) and (2) below, similar to the previous work.[7]

$$2H_2O \rightarrow 2O_2 + 4H^+ + 4e^- \quad \text{(Equation 1)}$$

$$4H_2O + 4e^- \rightarrow 2H_2 + 4OH^- \quad \text{(Equation 2)}$$

In chamber L, the generated H^+ reacted with $CaCO_3$ to release CO_2 and Ca^{2+}. The generated CO_2 could be converted to valuable carbonaceous products, and the Ca^{2+} migrated to the chamber R side and reacted with OH^-, producing $Ca(OH)_2$, as shown in Equations (3) and (4) below, similar to the work reported by Chiang et al.[7]

$$CaCO_3 + 2H^+ \rightarrow CO_2 + H_2O + Ca^{2+} \quad \text{(Equation 3)}$$

$$2Ca^{2+} + 2OH^- \rightarrow Ca(OH)_2 \quad \text{(Equation 4)}$$

Next, the current is switched to negative on electrode I (Figures 1C and 1E), process 2, where the CO_2 reduction process is carried out in chamber L, and the OER process is carried out in chamber R, as shown in Equations (5) and (6) below.

$$H_2O + nCO_2 + me^- \rightarrow C_xH_yO_z + OH^- \quad \text{(Equation 5)}$$

$$2H_2O \rightarrow 2O_2 + 4H^+ + 4e^- \quad \text{(Equation 6)}$$

Overall, by counting processes 1 and 2 together, the total reaction in the two-chamber can be illustrated with Equation (7).

$$mH_2O + xCaCO_3 \rightarrow xCa(OH)_2 + nH_2 + O_2 + C_xH_yO_z \quad \text{(Equation 7)}$$

Then, the process is repeated periodically to continuously produce $Ca(OH)_2$ and valuable carbonaceous products. If the pulse duration is enough, the $CaCO_3$ will be continuously converted into $Ca(OH)_2$. As the neutralization between the OH^- and H^+ in the system wastes energy, in order to enhance energy efficiency, it is necessary to optimize the generation and utilization of OH^- and H^+ by tuning the pulse duration.

To demonstrate the processes discussed above, a laboratory H-cell with two Au electrodes and Ar-saturated 1 M $NaClO_4$ was used as an electrochemical system. The detailed video of the entire electrochemical process in the two-chamber could be found in Video S1. The Au electrode has been reported as one of the best CO production electrocatalysts for electrochemical CO_2 reduction.[19] The glass microfiber filter papers (Whatman 1442-090) were chosen as the separator and placed between the two chambers to collect $Ca(OH)_2$. The Au wire electrode with a diameter of ~500 μm possesses a smooth surface in the microscopic view (Figure 2A). The X-ray diffraction (XRD) pattern reveals its polycrystalline crystal structure (Figure 2A), which is consistent with PDF#04–0784 Au. The positive current (i_p) was +30 mA, the negative current (i_n) was in the range of −1.5 ~ −5 mA, and the applied time of positive and negative current (t_p and t_n) was kept the same for 20 min. The detailed applied current and corresponding potentials were summarized in Figures S2A–S2E. The FE of CO is 6.8% when the negative current of −1.5 mA was applied to the Au electrode in chamber L. The FE of CO increases with the increasing applied current in the range of −1.5 ~ −3 mA. When −3 mA was applied, the FE of CO increased to 20%. The FE of CO started to decrease after the peak values at the applied current of −3 mA (Figure 2C and Table S1), which might be due to the mass transport limitation of CO_2.[20]

The stability test was carried out at the condition of i_p = +30 mA, i_n = −3 mA, t_p = t_n = 20 min in Ar-saturated 1 M $NaClO_4$ electrolyte for 7 cycles (Figure 2D). The FE of CO was stabilized at around 20% and the FE of H_2 was ~80% for 5 h (Figure 2E). After the stability test, the Au electrode was covered by $CaCO_3$, which was confirmed by the XRD pattern and scanning electron microscope (SEM) images (Figure S3). The $CaCO_3$ on the surface of the Au electrode either might be due to the reaction of Ca^{2+} with the generated CO_3^{2-} or the reaction of Ca^{2+} with HCO_3^- and OH^-.[7] Compared with the Au electrode tested in 1 M $NaClO_4$ electrolyte with $CaCO_3$, the Au tested in the same electrolyte without $CaCO_3$ only produces H_2 (Figure S4). This result demonstrated that the CO produced from the reduction of CO_2 generated from the decomposition of $CaCO_3$. Different from the pristine $CaCO_3$, the sample collected from the H-cell separator after the pulsed process is $Ca(OH)_2$, as confirmed by the XRD pattern (Figure 2F). Compared with $CaCO_3$, the morphology of $Ca(OH)_2$ collected after the electrochemical test shows a smaller size (Figure 2F). Besides $Ca(OH)_2$, there also exists a small amount of $CaCO_3$ in the collected sample from the separator, which might be formed upon exposure of the $Ca(OH)_2$ to air when preparing samples for XRD or contacted with the soluble CO_2 or HCO_3^- in the electrolyte (Figure 2F).

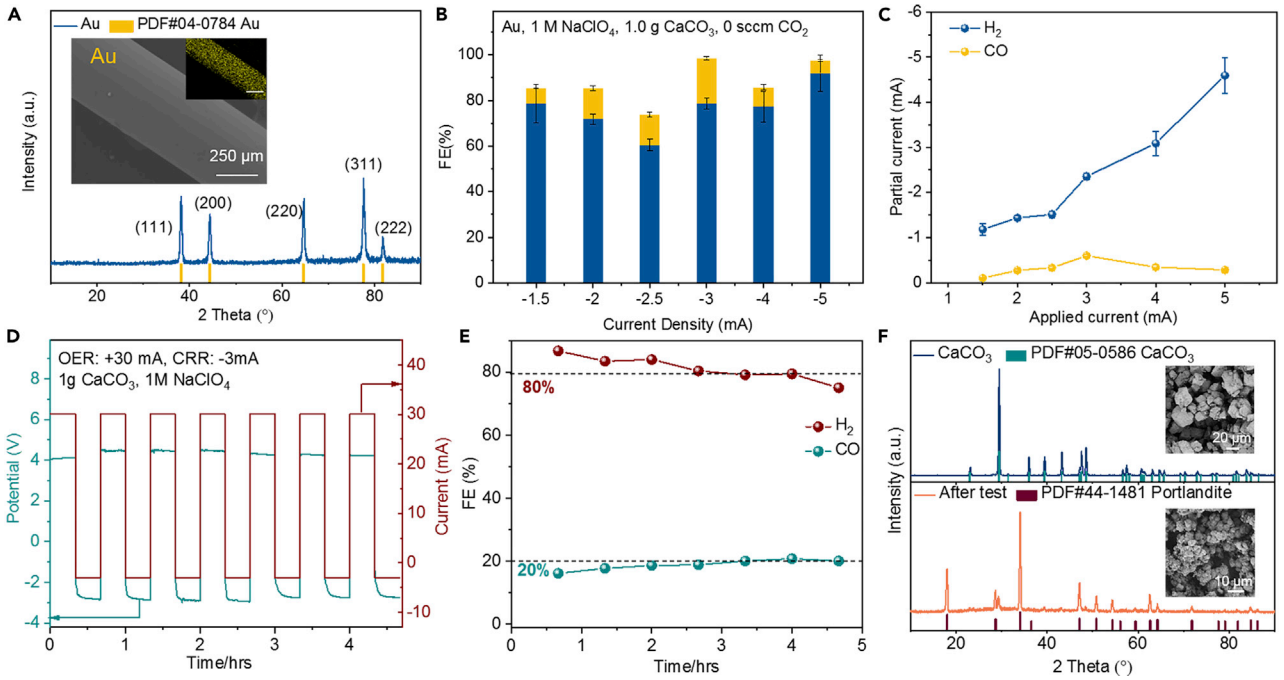

Figure 2. Characterization of the electrode, $CaCO_3$ and $Ca(OH)_2$, and electrochemical test in the two-chamber H-cell

(A) X-ray diffraction (XRD) patterns of pristine Au electrode, inset is scanning electron microscope (SEM) image and energy dispersive X-ray spectroscopy (EDX) mapping of Au electrode (the scale bar of mapping is 250 μm).

(B) Faradaic efficiency (FE) and (C) partial current density of CO and H_2 for the 1 M $NaClO_4$ electrolyte and 1g $CaCO_3$ with two Au electrodes (Every experiment was run for three times.).

(D) Positive and negative current pulsed performance of Au in 1 M $NaClO_4$ electrolyte and 1 g $CaCO_3$ with 7 cycles: i_o = +30 mA, i_r = −3 mA, t_o = t_r = 20 min, the applied current and corresponding potential.

(E) Faradaic efficiency (FE) of CO and H_2.

(F) X-ray diffraction (XRD) patterns and scanning electron microscope (SEM) images of $CaCO_3$ (above) and the samples in the middle of glass microfiber filter paper (below).

The electrode in the above-mentioned system carried out both electrochemical oxidation and reduction reactions, which required an oxidation stable electrode under positive currents. To expand the application of the concept of converting $CaCO_3$ into $Ca(OH)_2$ and valuable carbonaceous products, we further constructed an H-cell system with three chambers (Figure 3A). In this triple-chamber system, the OER process is separated from the CO_2 reduction process via two electrodes in one chamber, which make it applicable to nearly all kinds of CO_2 reduction electrodes. The detailed electrochemical test could be found in Video S2. In the triple-chamber system, Pt and Ir electrodes in chamber L and middle (M) chamber were used for HER and OER electrodes, respectively. The metal-based electrodes and NiFe layered double hydroxide (LDH) electrode in chambers M and L worked for CO_2 reduction and OER, respectively. To ensure the direct reduction of CO_2 generated from the decomposition of $CaCO_3$, the Ir electrode releasing H^+ and the metal electrode reducing CO_2 were settled in chamber M. Chamber L and M contain Ar-saturated 1 M $NaClO_4$ electrolyte, which is separated by glass microfiber filter paper. The chamber R contains Ar-saturated 1 M KOH electrolyte to construct a stable working environment for NiFe LDH, and it is separated from the chamber M via an anion exchange membrane.[3,21] First, a positive current of +30 mA was applied on the Ir electrode for 20 min to release H^+ for $CaCO_3$ decomposition. Then, the CO_2 generated from $CaCO_3$ decomposition was further reduced on the metal electrodes (Ag, In, Cu, and Cu nanowire electrodes) from −2 to −9 mA for 20 min.

We tested different metal electrocatalysts in the triple-chamber H-cell. As shown in Figure 3(B–D), the metal (Ag, In and Cu) wires with a diameter of ~500 μm were used as the electrodes. According to XRD patterns (Figure 3E), the metal electrodes are all polycrystalline. The NiFe LDH electrode (Figure S5) was used for the OER process in chamber R. The testing process was first carried out with 30 mA, where the Ir and Pt electrodes were used for the production of H^+ and OH^-, respectively. After 20 min water splitting,

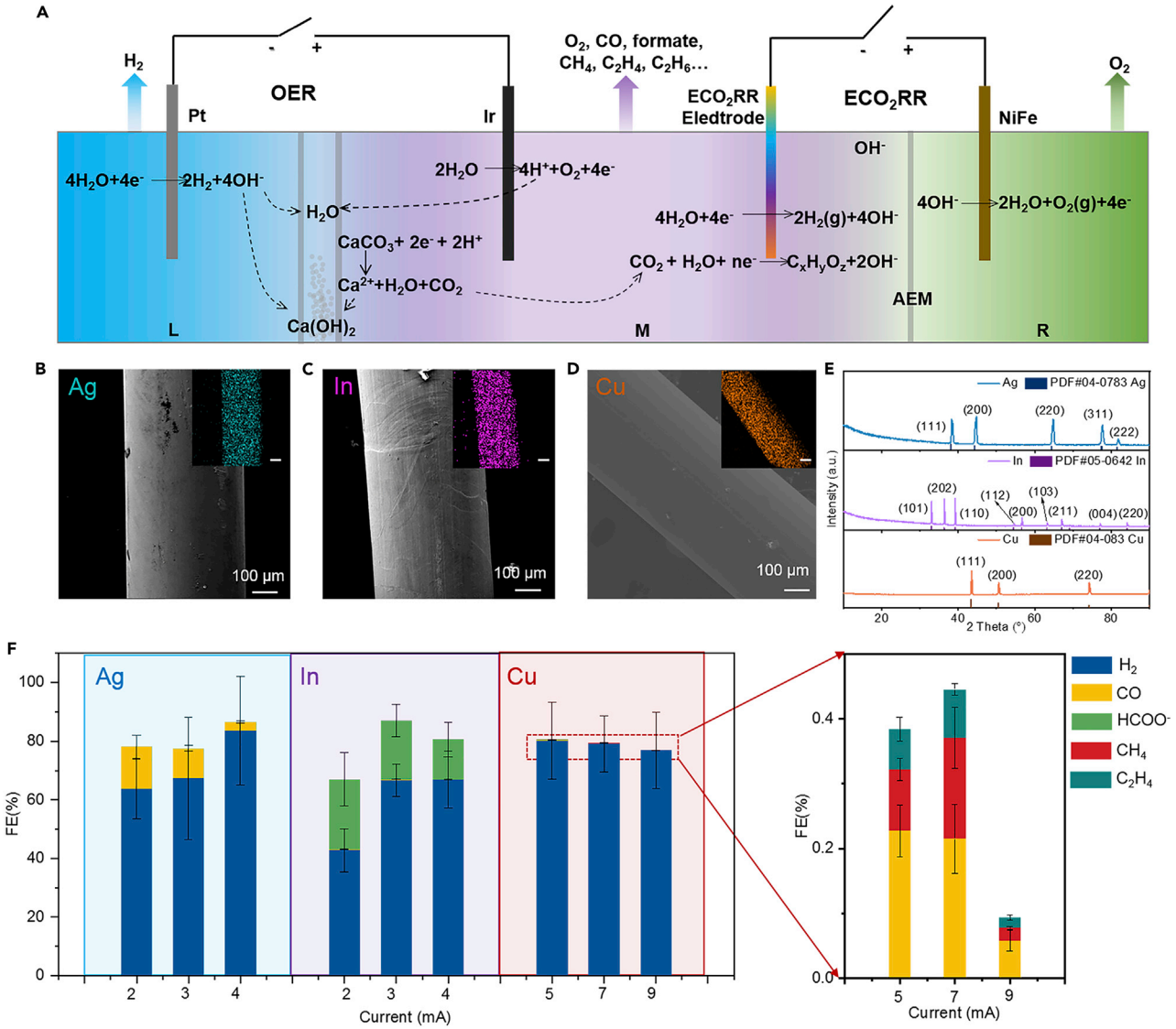

Figure 3. The detailed electrochemical reaction processes and electrochemical results in the triple-chamber H-cell

(A) Schematic illustration of the electrochemical conversion of $CaCO_3$ into $Ca(OH)_2$ and carbonaceous products process in the triple-chamber H-cell.

(B–D) Scanning electron microscope (SEM) images and energy dispersive X-ray spectroscopy (EDX) mapping of Ag, In, and Cu electrodes.

(E) X-ray diffraction (XRD) patterns of Ag, In, and Cu electrodes.

(F) The Faradaic efficiency (FE) of valuable carbonaceous products reduced in the 1 M $NaClO_4$ electrolyte and 1g $CaCO_3$ with the Ag, In, and Cu electrodes (Every experiment was run for three times.).

the $CaCO_3$ decomposed into Ca^{2+} and released CO_2. Then, a negative current was applied to Ag/In/Cu electrode for 20 min for CO_2 reduction. Here, the NiFe LDH was used as the anode. As illustrated in Figure 3F and S5, Ag achieved a peak FE of CO ~15% at −2 mA, In reached a peak FE of formate ~20%, and Cu produced CO, CH_4, and C_2H_4 (Figures 3F, S6 and Table S1). As the SEM images in Figure S7 shown, the metal electrodes after the test were covered with $CaCO_3$, which was confirmed by the XRD patterns (Figure S8). For instance, the Ag electrode after the test has both Ag (PDF#04–0783) and $CaCO_3$ (PDF#05–0586) diffraction peaks. Besides, we also tested the Cu nanowire electrode in the triple-chamber system. The nanowires have a length of ~5 μm (Figures S9A and S9B). According to the XRD patterns (Figure S10), the Cu nanowire electrode is polycrystalline. Through the test, we found that the Cu nanowire electrode produced CO, CH_4, C_2H_4, and C_2H_6 (Figure S11 and Table S1). However, the FEs for carbonaceous products of the Cu nanowire electrode are still low, which might be due to the dissolved Ca^{2+} in the solution, making the HER process dominate.[22] Similar to the three kinds of metal electrodes, the

surface of Cu nanowires was covered by $CaCO_3$, which was confirmed by SEM and XRD (Figures S9C, S9D, and S10). The $CaCO_3$ on the surface of the electrodes only reflects the state after the CO_2 reduction process, and it is only a small amount. As long as we prolong the pulse duration, the $CaCO_3$ will be continuously converted into $Ca(OH)_2$. To confirm the carbonaceous products were generated from $CaCO_3$, we further tested the Ag/In/Cu metal electrodes in the Ar-saturated 1 M $NaClO_4$ electrolyte without $CaCO_3$ with the same electrochemical method. Except for H_2, no CO_2 reduction product was detected (Figure S12), which indirectly confirmed that $CaCO_3$ was the carbon source of the carbonaceous products.

The overall electrochemical process is complicated. Therefore, we calculated the energy efficiency of the system by separating the two electrochemical processes in the water splitting process and the electrochemical CO_2 reduction process. Through the rough calculation (the detailed calculation process could be found in supporting information), we found that the energy efficiency (EE) of the water splitting process was 26.17%, the EE of the electrochemical CO_2 reduction process was ~24%–80%, and the overall EE of the system is ~25%–28%. The energy efficiencies were summarized in Tables S2 and S3. The energy efficiency of this system shows the potential of converting the limestone into portlandite and valuable carbonaceous products.

Conclusion

In conclusion, we demonstrate an *in situ* electrochemical process to transform $CaCO_3$ into $Ca(OH)_2$. Moreover, this design enables *in situ* conversion of CO_2 during cement production, which converts the CO_2 into valuable carbonaceous products, such as CO, formate, methane, ethylene, and ethane. By integrating electrochemical water splitting and CO_2 reduction with the chemical decomposition of $CaCO_3$, our electrochemical system demonstrates a proof of concept to produce cement in a green and renewable manner. To promote the application of our design in industrial cement production, we propose the following perspectives: (i) Developing efficient catalysts and optimizing system design will further improve the FE of carbonaceous products; (ii) Considering the neutralization between the OH^- and H^+ in the system and the CO_2 solubility, it is necessary to optimize the generation and utilization of OH^- and H^+ by tuning the pulse duration for improving the efficiencies; (iii) An industrially relevant flow electrolyzer should be designed to improve the utilization rate of CO_2 in the system, fully considering the introduction of $CaCO_3$ and the separation of $Ca(OH)_2$. Our work provides a green and sustainable path for cement production, which will complement the existing CO_2 reduction technologies and help to build a carbon-neutral society.

Limitations of the study

Our work demonstrates the proof of concept to convert $CaCO_3$ into $Ca(OH)_2$ and valuable carbonaceous products in an integrated system. Nevertheless, there are still some issues to tackle before industrial application. Owing to the low CO_2 solubility in water, the current system only runs at low current densities, and parts of the CO_2 released from $CaCO_3$ decomposition may be released in the gaseous form. In the future, an industrially relevant flow cell system should be developed to improve the utilization of CO_2 and the production rate. In addition, the continuous supply of solid calcium carbonate to the system and the separation of $Ca(OH)_2$ from the system should also be considered.

STAR★METHODS

Detailed methods are provided in the online version of this paper and include the following:

- KEY RESOURCES TABLE
- RESOURCE AVAILABILITY
  - Lead contact
  - Materials availability
  - Data and code availability
- EXPERIMENTAL MODEL AND SUBJECT DETAILS
  - Chemicals
  - Preparation of the metal electrodes
  - Preparation of the NiFe layered double hydroxide (LDH) electrodes
  - Material characterizations
  - Electrochemical measurements and products
  - Electrochemical reaction in the two-chamber H-cell
  - Electrochemical reaction in the triple-chamber H-cell

- Calculation of Faradaic Efficiencies (FE)
- Calculation of energy efficiencies (EE)
- Calculation of the theoretical extent of $CaCO_3$ decomposition

SUPPLEMENTAL INFORMATION

Supplemental information can be found online at https://doi.org/10.1016/j.isci.2023.106015.

ACKNOWLEDGMENTS

J.L. acknowledges the funding support from the National Key Research and Development Program of China (2019YFE0123400), the Excellent Young Scholar Fund from the National Science Foundation of China (22122903), the Tianjin Distinguished Young Scholar Fund (20JCJQJC00260), and the Haihe Laboratory of Sustainable Chemical Transformations.

AUTHOR CONTRIBUTIONS

J.L. conceived and supervised the project. Q.X. carried out the experiment. J.L. and Q.X. wrote the manuscript. All authors discussed the results and contributed to the manuscript.

DECLARATION OF INTERESTS

Q.X. and J.L. filed a patent application regarding the electrochemical process and its application reported in this work.

Received: December 9, 2022
Revised: January 4, 2023
Accepted: January 13, 2023
Published: January 20, 2023

REFERENCES

1. Hausfather, Z., Marvel, K., Schmidt, G.A., Nielsen-Gammon, J.W., and Zelinka, M. (2022). Climate simulations: recognize the 'hot model'problem. Nature Publishing Group, *26–29*.

2. Alkama, R., Forzieri, G., Duveiller, G., Grassi, G., Liang, S., and Cescatti, A. (2022). Vegetation-based climate mitigation in a warmer and greener World. Nat. Commun. *13*, 606.

3. Luo, J., Im, J.-H., Mayer, M.T., Schreier, M., Nazeeruddin, M.K., Park, N.-G., Tilley, S.D., Fan, H.J., and Grätzel, M. (2014). Water photolysis at 12.3% efficiency via perovskite photovoltaics and Earth-abundant catalysts. Science *345*, 1593–1596.

4. Huang, J.E., Li, F., Ozden, A., Sedighian Rasouli, A., García de Arquer, F.P., Liu, S., Zhang, S., Luo, M., Wang, X., Lum, Y., et al. (2021). CO_2 electrolysis to multicarbon products in strong acid. Science *372*, 1074–1078.

5. Fennell, P.S., Davis, S.J., and Mohammed, A. (2021). Decarbonizing cement production. Joule *5*, 1305–1311.

6. Rocha, J.H.A., Toledo Filho, R.D., and Cayo-Chileno, N.G. (2022). Sustainable alternatives to CO_2 reduction in the cement industry: a short review. Mater. Today Proc. *57*, 436–439.

7. Ellis, L.D., Badel, A.F., Chiang, M.L., Park, R.J.Y., and Chiang, Y.-M. (2020). Toward electrochemical synthesis of cement-An electrolyzer-based process for decarbonating $CaCO_3$ while producing useful gas streams. Proc. Natl. Acad. Sci. USA *117*, 12584–12591.

8. Benhelal, E., Shamsaei, E., and Rashid, M.I. (2021). Challenges against CO_2 abatement strategies in cement industry: a review. J. Environ. Sci. *104*, 84–101.

9. Rumayor, M., Fernández-González, J., Domínguez-Ramos, A., and Irabien, A. (2022). Deep Decarbonization of the Cement Sector: a Prospective Environmental Assessment of CO_2 Recycling to Methanol. et al. ACS Sustain. Chem. Eng. *10*, 267–278.

10. Perego, A., Kulkarni, D., Chang, H.-M., Wang, X., Wei, J., Li, M., and Zenyuk, I.V. (2021). Electrochemical flow reactor for cement clinker production. Meet. Abstr. *02*, 840.

11. Zhou, C., Ni, J., Chen, H., and Guan, X. (2021). Harnessing electrochemical pH gradient for direct air capture with hydrogen and oxygen by-products in a calcium-based loop. Sustain. Energy Fuels *5*, 4355–4367.

12. Lees, E.W., Goldman, M., Fink, A.G., Dvorak, D.J., Salvatore, D.A., Zhang, Z., Loo, N.W.X., and Berlinguette, C.P. (2020). Electrodes designed for converting bicarbonate into CO. ACS Energy Lett. *5*, 2165–2173.

13. Li, T., Lees, E.W., Zhang, Z., and Berlinguette, C.P. (2020). Conversion of bicarbonate to formate in an electrochemical flow reactor. ACS Energy Lett. *5*, 2624–2630.

14. Salvatore, D.A., Weekes, D.M., He, J., Dettelbach, K.E., Li, Y.C., Mallouk, T.E., and Berlinguette, C.P. (2018). Electrolysis of gaseous CO_2 to CO in a flow cell with a bipolar membrane. ACS Energy Lett. *3*, 149–154.

15. Salvatore, D., and Berlinguette, C.P. (2020). Voltage matters when reducing CO_2 in an electrochemical flow cell. ACS Energy Lett. *5*, 215–220.

16. Zhang, Z., Lees, E.W., Habibzadeh, F., Salvatore, D.A., Ren, S., Simpson, G.L., Wheeler, D.G., Liu, A., and Berlinguette, C.P. (2022). Porous metal electrodes enable efficient electrolysis of carbon capture solutions. Energy Environ. Sci. *15*, 705–713.

17. Zhang, Z., Mowbray, B.A.W., Parkyn, C.T.E., Waizenegger, C., Williams, A.S.R., Lees, E.W., Ren, S., Kim, Y., Jansonius, R.P., and Berlinguette, C.P. (2022). Cement clinker precursor production in an electrolyser. Energy Environ. Sci. *15*, 5129–5136.

18. Barbero-Barrera, M.M., Gomez-Villalba, L.S., Ergenç, D., Sierra-Fernández, A., and Fort, R. (2022). Influence of curing conditions on the mechanical and hydric performance of air-lime mortars with nano-$Ca(OH)_2$ and nano-SiO_2 additions. Cem. Concr. Compos. *132*, 104631.

19. Feaster, J.T., Shi, C., Cave, E.R., Hatsukade, T., Abram, D.N., Kuhl, K.P., Hahn, C., Nørskov, J.K., and Jaramillo, T.F. (2017). Understanding selectivity for the

electrochemical reduction of carbon dioxide to formic acid and carbon monoxide on metal electrodes. ACS Catal. *7*, 4822–4827.

20. Wang, X., Xu, A., Li, F., Hung, S.-F., Nam, D.-H., Gabardo, C.M., Wang, Z., Xu, Y., Ozden, A., Rasouli, A.S., et al. (2020). Efficient methane electrosynthesis enabled by tuning local CO_2 availability. J. Am. Chem. Soc. *142*, 3525–3531.

21. Luo, J., Vermaas, D.A., Bi, D., Hagfeldt, A., Smith, W.A., and Grätzel, M. (2016). Bipolar membrane-assisted solar water splitting in optimal pH. Adv. Energy Mater. *6*, 1600100.

22. Monteiro, M.C.O., Dattila, F., López, N., and Koper, M.T.M. (2022). The role of cation acidity on the competition between hydrogen evolution and CO_2 reduction on gold electrodes. J. Am. Chem. Soc. *144*, 1589–1602.

23. Luo, J., Steier, L., Son, M.-K., Schreier, M., Mayer, M.T., and Grätzel, M. (2016). Cu_2O nanowire photocathodes for efficient and durable solar water splitting. Nano Lett. *16*, 1848–1857.

24. Lai, W., Qiao, Y., Zhang, J., Lin, Z., and Huang, H. (2022). Design strategies for markedly enhancing energy efficiency in the electrocatalytic CO_2 reduction reaction. Energy Environ. Sci. *15*, 3603–3629.

STAR★METHODS

KEY RESOURCES TABLE

REAGENT or RESOURCE	SOURCE	IDENTIFIER
Chemicals, peptides, and recombinant proteins		
$CaCO_3$	Aladdin	CAS no. 471-34-1
$NaClO_4$	Aladdin	CAS no. 7601-89-0
$Ni(NO_3)_2{\cdot}6H_2O$	Aladdin	CAS no.13478-00-7
$Fe(NO_3)_3{\cdot}9H_2O$	Aladdin	CAS no.7782-61-8
$CO(NH_2)_2$	Aladdin	CAS no. 57-13-6
KOH	Aladdin	CAS no.1310-58-3
Au wires	Zhongnuo New Material Co., Ltd.	Au144014
Ag wires	Guantai Metal Materials Co., Ltd.	Ag 0.5 mm
In wires	Guantai Metal Materials Co., Ltd.	In 0.5 mm
Cu wires	Guantai Metal Materials Co., Ltd.	Cu 0.5 mm
Cu Foil	Hujiang Shanghai Co., Ltd.	Cu 0.3 mm
Other		
Gas Chromatograph	Thermo GC 1310	https://www.thermofisher.cn/order/catalog/product/GHA000010011?SID=srch-srp-GHA000010011
Liquid Chromatograph	Agilent 1260 Infinity	https://www.agilent.com.cn/zh-cn/product/liquid-chromatography/hplc-systems/analytical-hplc-systems/1260-infinity-ii-lc-system
Electrochemical workstation	Autolab, PGSTAT101	http://www.metrohm17.com/forestsun-Products-16042560/
Scanning Electron Microscope	FEI NanoSEM650	https://www.memphis.edu/imc/microscopy/nova-nano.php
X-ray diffraction	Rigaku D/MAX-2500	https://www.rigaku.com/products/xrd/smartlab

RESOURCE AVAILABILITY

Lead contact

Further information and requests for resources should be directed to and will be fulfilled by the lead contact, Jingshan Luo (jingshan.luo@nankai.edu.cn).

Materials availability

All materials generated in this study are available from the lead contact without restriction.

Data and code availability

- All data reported in this paper will be shared by the lead contact upon request.
- This paper does not report original code.
- Any additional information required to reanalyze the data reported in this paper is available from the lead contact upon request.

EXPERIMENTAL MODEL AND SUBJECT DETAILS

Chemicals

All the chemicals including $CaCO_3$ (99.99%), $NaClO_4$ (99.99%), $Ni(NO_3)_2{\cdot}6H_2O$ (99%), $Fe(NO_3)_3{\cdot}9H_2O$ (98%), $CO(NH_2)_2$ (99-100.5%), KOH (99.99%) were of analytical grade and used without further purification.

Preparation of the metal electrodes

All the metal electrodes (including Au, Ag, In, Cu, the purity is 99.999%) used in these experiments are 0.5 μm. Before preparing the 0.78 cm^{-2} electrodes with the length of 5 cm, all the metal wires were washed sequentially via CH_3CH_2OH, deionized water, dilute HCl and deionized water. Cu Nanowires (Cu NWs) electrodes were synthesized by electrochemical pre-reduce the anodic oxidized $Cu(OH)_2$, like previous report.[23] The Cu foil (99.999%) was cleaned by ultrasonic in ethanol, diluted HCl, DI water and dried under Ar flow. The Cu foil was anodized in 3.0 mol/L KOH aqueous electrolyte at a constant current density of 10 mA cm^{-2} until the current gradually stabilizes to form $Cu(OH)_2$ nanowire arrays. Then the $Cu(OH)_2$ nanowire @ Cu Foil electrodes were pre-reduced to form Cu nanowires under a negative current via electrochemical methods.

Preparation of the NiFe layered double hydroxide (LDH) electrodes

NiFe LDH was synthesized by a hydrothermal method. In this experiment, we synthesized NiFe LDH with the Ni:Fe ratio of ~3:1. Briefly, 0.75 mmol $Ni(NO_3)_2{\cdot}6H_2O$, 0.25 mmol $Fe(NO_3)_3{\cdot}9H_2O$, and 5 mmol $CO(NH_2)_2$ were dissolved in 35 mL of deionized water and stirred to form a clear solution. Ni foam (about 3 cm×4 cm each) was carefully treated with CH_3CH_2OH, deionized water, dilute HCl and deionized water. The above solution and Ni foam were then transferred to a 50 mL Teflon-lined stainless-steel autoclave, sealed, and maintained at 120 °C for 12 h. This was then allowed to cool to room temperature naturally. The pale brown NiFe LDH samples were then put into deionized water/ethanol, sonicated for 5 min, and then dried at 80 °C for 6 h.

Material characterizations

The size and morphologies of as-prepared electrodes were characterized by a field-emission scanning electron microscope (SEM, FEI NanoSEM650) operating at 20 kV. X-ray diffraction (XRD) patterns were collected on Rigaku D/MAX-2500 XRD with Cu Kα radiation (40 kV, 40 mA, λ = 1.5418 Å), recorded with 2θ ranging from 5° to 90°, 10°/min.

Electrochemical measurements and products

The electrochemical measurements were carried out at room temperature in a two-chamber H-cell and a triple-chamber H-cell using an electrochemical workstation (Autolab, PGSTAT101). The gas products were detected via gas chromatograph (Thermo GC 1310), and the liquid products were detected via high performance liquid chromatograph (HPLC, Agilent 1260 Infinity). There exists a thermal conductivity detector (TCD) and two flame ionization detectors (FID) in the GC, which are used for the analysis of H_2 and carbon containing products, such as CH_4, CO, C_2H_4 and C_2H_6, etc. Here, the gas products were collected with an injector, and 5 mL of gas was taken and injected into the GC. The three quantitative loops of the gas chromatograph are 1 mL, 1 mL, and 500 uL respectively. Therefore, the gas taken can be filled and quantitatively filled, which ensures the accuracy of the test. For the liquid products, we used variable wavelength detector (VWD) in the HPLC to detect formate. The collected liquid products, containing 900 μL electrolytes acidified with 100 μL 4.5 M sulfuric acid, were quantified by the HPLC. Moreover, every experiment has been run for three times.

Electrochemical reaction in the two-chamber H-cell

The cement electrolyzer reported by Ellis et al. could produce the $Ca(OH)_2$ and CO_2 via $CaCO_3$ electrolysis.[7] Based on this work, we integrated the $Ca(OH)_2$ formation process with electrochemical CO_2 reduction process in the two-chamber H-cell. This system could realize the conversion of $CaCO_3$ into $Ca(OH)_2$ and valuable carbonaceous products simultaneously. As shown in Figure 1, the Au electrodes were chosen as electrodes both in left chamber (L) and right chamber (R) in the two-chamber H-cell. The chamber L as shown Figure 1 contains 1 g $CaCO_3$ with 1 M $NaClO_4$ electrolyte. First, the positive current of +30 mA was applied to the electrode I in chamber L for 20 min. During this process, the oxygen evolution reaction (OER) and the hydrogen evolution reaction (HER) happened in the chamber L and chamber R, respectively. The H^+ generated in chamber L during OER process would react with $CaCO_3$ to release CO_2 and Ca^{2+}, and the generated Ca^{2+} would migrate and react with OH^- generated in chamber R to form $Ca(OH)_2$. Then, the applied current was reversely switched to -1.5 mA, -2.0 mA, -2.5 mA, -3 mA, -4 mA and -5 mA for 20 min, respectively. In this case, the electrochemical CO_2 reduction process would happen in chamber L and the OER process would happen in chamber R. The electrochemical CO_2 reduction process would happen in chamber L and OER process would happen in chamber R. During the experiment, positive and negative

currents were applied alternately on the same electrode. In this two-chamber H-cell, our design could realize the reaction process by switching positive and negative currents, and in-situ convert $CaCO_3$ to $Ca(OH)_2$ and valuable carbonaceous products.

Electrochemical reaction in the triple-chamber H-cell

To further expand the application of this system, we designed a triple-chamber H-cell, in which the CO_2 reduction electrode and OER electrode were different and separated. As shown in Figure 3, the Middle chamber (M) contains $CaCO_3$ with 1 M $NaClO_4$ electrolyte, which is separated with glass microfiber filter paper (whatman 1442-090). The commercial Pt and Ir electrodes were chosen as electrodes in chamber Left (L) and chamber Right (R), respectively. The chamber R containing with 1 M KOH was separated from chamber M via an anion exchange membrane (AEM), and the highly efficient CO_2 reduction electrodes and NiFe LDHs electrodes were used as electrodes in chambers M and R respectively. First, the positive current of +30 mA was applied to the Ir electrode in chamber M for 20 min. During this process, the HER process and OER process happened in chamber L and chamber M, respectively. The H^+ generated during OER process would react with $CaCO_3$ to release CO_2 and Ca^{2+}, and the generated Ca^{2+} would migrate and react with OH^- generated in chamber L to form $Ca(OH)_2$. Then, the different negative currents were applied to the CO_2 electrode in the chamber M for 20 min, and the CO_2 generated in chamber M would be reduced. The design of the triple-chamber H-cell could be further used for all kinds of CO_2 reduction electrodes, which would not be limited by the electrochemical corrosion caused by switching to the positive and negative currents.

Calculation of Faradaic Efficiencies (FE)

The FE for gas and liquid products were calculated based on the below Equation (8):

$$FE(\%) = \frac{Q_{product}}{Q_{total}} \times 100\% \quad \text{(Equation 8)}$$

$Q_{product}$ and Q_{total}: the charge transferred for product formation and charge passed through the working electrode.

Combining the above equation and the actual situation, the detailed calculation for Faradaic Efficiencies of CO_2 products could be calculated through the Equation (9) as below:

$$FE(\%) = \frac{n \times C_{product(gas)}}{I \times t} \times 100\% \quad \text{(Equation 9)}$$

$C_{product}$ and n: the concentration of the products measured by GC and the number of electrons required for producing one molecule of the related products.

t: tested time; I: current.

Calculation of energy efficiencies (EE)

The electrochemical transformation process reported in this work, includes the neutral water splitting process and electrochemical CO_2 reduction process, which is complicated. To better evaluate the energy efficiency of this device, we calculated the energy efficiency of the two-step electrochemical processes separately.

For the first step, water splitting process, the efficiency was calculated as follow[24]:

$$EE_w(\%) = \Delta E_W^0 \Big/ \Delta E_W^{Applied} \times FE \quad \text{(Equation 10)}$$

ΔE_W^0: equilibrium full cell potential, $E_{HER}^0 - E_{OER}^0 = 0 - 1.23 = -1.23$ V
$\Delta E_W^{Applied}$: The applied potential at 30 mA is ~4.7 V.

The products of the water splitting process are mainly H_2 and O_2, we assumed their FE is 100%, therefore the energy efficiency at 30 mA current condition could be calculated as:

$$EE_w(\%) = 1.23/4.7 \times 100\% = 26.17\%$$

For the second step, electrochemical CO_2 reduction process. the efficiency was calculated as follow and summarized in Table S1.

$$EE_C(\%) = \Delta E_C^0 \Big/ \Delta E_C^{Applied} \times FE \quad \text{(Equation 11)}$$

ΔE_C^0: equilibrium full cell potential, e.g.: $E_{CO2/CO}^0 - E_{OER}^0 = -0.11 - 1.23 = -1.34\,V$

$\Delta E_C^{Applied}$: the applied cell potential at different reduction current.

The overall energy efficiency of the device could be calculated as follow and summarized in Table S2.

$$EE_D(\%) = \left(\Delta U_w^{Input} \times EE_w(\%) + \Delta U_C^{Input} \times EE_C(\%)\right) \Big/ \left(\Delta U_w^{Input} + \Delta U_C^{Input}\right) \quad \text{(Equation 12)}$$

ΔU_w^{Input}: Full cell energy of water splitting process, $\Delta U_w^{Input} = \Delta E_w^{Input} \times \Delta I_w^{Input} \times \Delta t_w^{Input}$

ΔU_C^{Input}: Full cell energy of electrochemical CO2 reduction process.

Calculation of the theoretical extent of $CaCO_3$ decomposition

Assuming all the generated H^+ reacted with the $CaCO_3$, as the amount of the generated H^+ is equal to the amount of e^-, the extent of $CaCO_3$ decomposition can be calculated via the following equations:

$$Q = It$$

$$n_e = Q/e \times N_A$$

$$m_{CaCO3} = n_e/2 \times M_{CaCO3}$$

Q: Electricity, C;

e: 1.6×10-19 C;

NA: 6.022×10^{23};

Here, the current is 30 mA, the time is 1200 s, and the detailed calculation process was as follows:

$$Q = It = 30 \times 1200/1000 = 36\ C$$

$$n_e = Q/e \times N_A = 36/\left(36 \times 10^{-19}\right) \times 6.022 \times 10^{23} = 0.000598007\ mol$$

$$m_{CaCO3} = n_e/2 \times M_{CaCO3} = 0.000598007 \times 100.0869 \times 1000 = 29.93\ mg$$